ELSEVIER

Journal of Hydrology 194 (1997) 107–125

Journal of Hydrology

A relative-flux-correction scheme for analyzing three dimensional data of a tile-drained agricultural plot[1]

B.P. Mohanty[a,*], R.S. Kanwar[b]

[a]*US Salinity Laboratory USDA-ARS, Riverside, California, USA*
[b]*Agricultural and Biosystems Engineering Iowa State University, Ames, Iowa, USA*

Received 18 September 1995; revised 24 April 1996; accepted 12 June 1996

Abstract

The use of simple geostatistical tools is often constrained by data trend (nonstationarity) to characterize the spatial variability of soil properties in the subsurface environment influenced by any site-specific feature(s). Adaptive approaches, such as site-specific robust-resistant schemes, median polishing, trend analysis, etc., are thus used to preprocess the spatial data before analyzing for their spatial structures. Soil water nitrate–nitrogen (NO_3–N) concentration (mg l^{-1}) and soil moisture content (cm) data collected jointly from 175 sites arranged on a $5 \times 7 \times 5$ three-dimensional (3-D) grid network of 7.6 m $\times$ 7.6 m $\times$ 0.3 m spacings in a tile-drained agricultural plot were analyzed for their three-dimensional spatial distribution and for possible coregionalization. We propose a physical process-based correction scheme to preprocess the nonstationary spatial data of soil NO_3–N concentration and soil moisture content. Using the subsurface-drain flow phenomenon, we developed a relative-Darcy-flux-based correction scheme to remove any tile drainage-induced nonstationarity in the spatial data of soil NO_3–N concentration and soil moisture content prior to conducting the spatial analysis in the 3-D soil volume. 3-D composite semivariograms of relative-flux-corrected NO_3–N concentration and relative-flux-corrected moisture content showed anisotropic linear structures in three principal directions. Linear models characterized by steep slopes were found in the directions perpendicular to tile line as opposed to nugget models found in the direction parallel to the tile line. Good spatial correlation between the relative-flux-corrected NO_3–N concentration and relative-flux-corrected soil moisture content and their anisotropic linear semivariograms produced anisotropic linear cross semivariograms in 3-D. The 3-D composite cross

* Corresponding author.

[1]Journal Paper No. J-15064 of the Iowa Agriculture and Home Economics Experiment Station, Ames, Iowa 50011. Project No. 2988.

PII S0022-1694(96)03225-8

semivariogram will be useful in predicting the more expensive variable, (relative-flux-corrected) soil water NO_3–N concentration, at unsampled locations in the soil profile with a cheaper surrogate, the measured (relative-flux-corrected) soil moisture content.

1. Introduction

Water quality research has intensified in recent years because of the environmental effects of transport of agrochemicals to groundwater. Effective and inexpensive ways of determining nitrate concentration in the soil profile and in groundwater are needed to develop methods for controlling water pollution problems. Transport, transformation, and distribution of nitrate–nitrogen (NO_3–N) depend on the site-specific physical, chemical and biological processes occurring in the three-dimensional (3-D) soil profile of variably deep unsaturated and saturated zones. Examples of these processes responsible for the spatial distribution of NO_3–N are water and solute displacement under variably-saturated non-steady flow conditions along preferential and nonpreferential flow paths, including site-specific subsurface-drainage-induced flows to tile lines and agricultural drainage wells, variable water table depth causing nitrification and denitrification, nitrogen transformations by enzymatic and bacterial pathways, plant uptake of water and nitrogen, and soil properties (Wagenet and Rao, 1983). As described by Beek and Frissel (1973) and Kanwar et al. (1983), nitrogen transport in the soil is caused by mass transport of water (advection) and diffusion and dispersion. Diffusion is a function of the concentration gradient, but dispersion and mass transport are proportional to the mass flow rate of water through the soil profile and nitrate concentration gradient. Because, under both saturated and unsaturated conditions, water is the major carrier for nitrate transport through the soil profile, variability of (residual) soil nitrate concentration could be expected to have spatial correlation with that of the (resident) soil moisture content and water flux moving across the (sample) soil volume. When NO_3–N sampling is an expensive monitoring protocol to address water quality issues in problem areas, the labor and expenses involved could increase with spatial extent of the problem. A way to cut down the labor and expense would be to find a cheaper surrogate that can estimate the NO_3–N concentration at unsampled locations with reasonable precision. As per the coregionalization theory (Journel and Huijbregts, 1978), this will only be true when the primary variable and the co-variates show reasonably good spatial correlations and spatial structures. Butters et al. (1989) and White et al. (1986), have proposed a convenient method for assessing the lateral variability of the solute movement. They suggested examining the spatial distribution of the so-called solute transport volume, or equivalently the pore volume water content.

Subsurface tile drainage is a common agricultural practice to get rid of excessive wetness in the shallow soil profiles in many parts of the United States. Several researchers (Baker et al., 1975; Baker et al., 1989; Kanwar et al., 1988; Kanwar and Baker, 1991; Mohanty and Kanwar, 1994) have studied the accumulation and/or spatial distribution of

NO_3–N in soil profiles and NO_3–N loss with tile drainage water under continuous corn. Although several physical, chemical, and biological processes are involved in the transport and transformation of nitrogen fertilizer in the tile-drained soil profile, tile lines located at a certain depth govern the major site-specific saturated flow and transport pattern. In this paper, we propose a knowledge-based site-specific relative-Darcy-flux-based correction to remove the tile-drainage-induced trend of certain concurrent saturated flow from the spatial data of soil NO_3–N concentration and soil moisture content in a tile-drained plot. The homogenized residual variables could be successfully analyzed for three-dimensional spatial variability.

In recent years, geostatistical techniques (Journel and Huijbregts, 1978) have been used extensively to study the spatial behavior of various soil properties in the shallow surface layers (Mohanty and Kanwar, 1994; Mohanty et al., 1994a; Mohanty et al., 1991; Yates and Warrick, 1987; Trangmar et al., 1986a; Trangmar et al., 1986b) as well as deeper aquifers (Woodbury and Sudicky, 1991; Ahmed and De Marsily, 1987). In a recent study (Mohanty and Kanwar, 1994), we presented a 'generic' three-dimensional median polishing scheme to preprocess nonstationary spatial data collected in a three-dimensional grid, where NO_3–N concentration data were approximated by an additive model consisting of a mean component (μ), components in three principal (x-, y-, and z-) directions (α_i, β_j, and ξ_k), components in diagonal directions ($g\ (x_i - \overline{x})(y_j - \overline{y})$), and a random component (ϵ_{ijk}). Removing the directional components and the mean component by using the three-dimensional median polishing scheme left the random component behind, which was analyzed to find the tillage-induced spatial structure of NO_3–N concentration in the soil profile. In this paper, we propose a more 'case-specific' physical process-based correction scheme to preprocess the three-dimensional nonstationary spatial data of NO_3–N concentration and soil moisture content (caused by certain concurrent saturated (tile) flow) within a tile-drained soil profile before the three-dimensional spatial analysis. The objective of this study is to use the site-specific spatial information and the involved concurrent major physical processes leading to a 'knowledge-based' spatial analysis for soil NO_3–N concentration and soil moisture content in a 3-D soil volume.

2. Experimental design

A 0.4 ha plot was selected for this study at the Agronomy and Agricultural Engineering Research Center near Ames, Iowa. This plot had been under the same conventional tillage system for the last 5 years and had received an annual application of 175 kg ha^{-1} of liquid nitrogen fertilizer immediately after planting for continuous corn production. Soils were Nicollet (fine-loamy, mixed, mesic Aquic Hapludoll) and Clarion (fine-loamy, mixed mesic Typic Hapludoll) loams in the Clarion–Nicollet–Webster Association with a maximum slope of 2%. Physical properties of the experimental site can be found elsewhere (Mohanty et al., 1994b). After heavy storm events, the shallow ground water table in this field occasionally rises close to the soil surface. The plot was drained by a single subsurface tile drain laid at about 120 cm depth (Fig. 1).

Soil samples were collected according to a $5 \times 7 \times 5$ three-dimensional grid network of 175 sites with a regular grid spacing of 7.6 m (in x-direction), 7.6 m (in y-direction), and

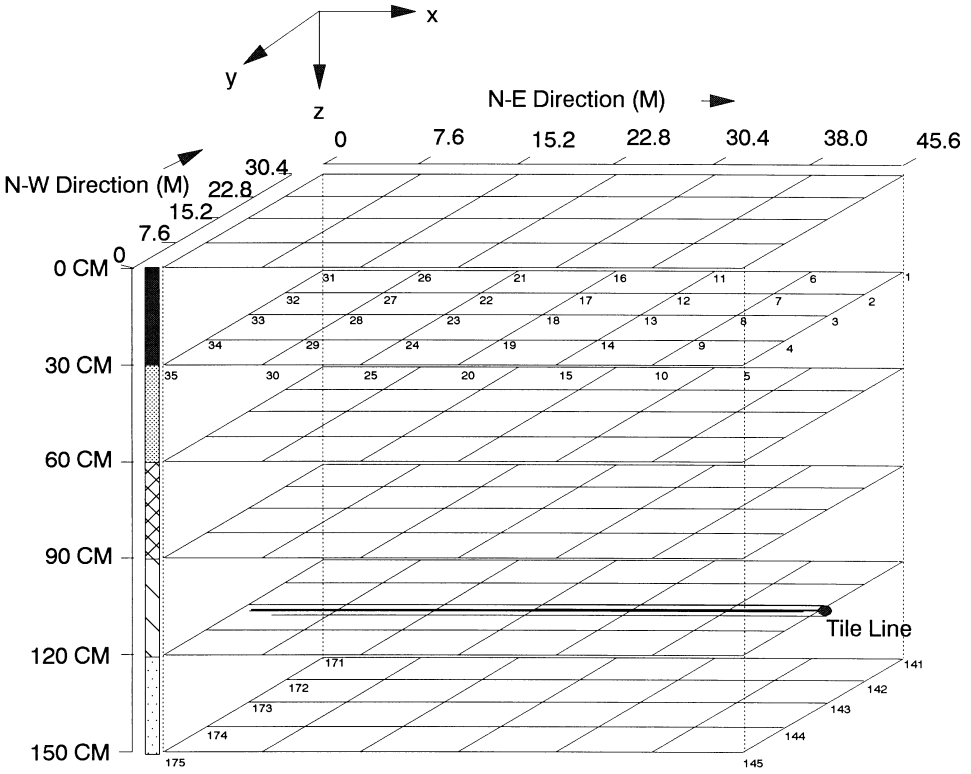

Fig. 1. (a) Arrangement of sampling locations in the experimental plot. 175 sites arranged on a $7 \times 7 \times 5$ grid. 10 cm long soil sample at each site was used for soil NO_3–N concentration and soil moisture content analysis. A tile line is located at 120 cm depth in the center of the plot to drain periodic excessive wetness.

0.3 m (in *z*-direction) as shown in Fig. 1. This grid was designed symmetrically across the drainage tile (in *y*-direction). At the center of the plot, soil samples were taken adjacent to the tile line. The sampling plan was adapted considering the geostatistics practical rule of minimum number of samples (30) (Journel and Huijbregts, 1978, pp. 194; Cressie, 1993), and labor and budget limitations. Four different soil sampling devices, a 20.3 cm power earth auger, a 5.1 cm hand earth auger, a 3.2 cm soil probe, and a 1.9 cm soil probe, were used with a secondary objective to evaluate the effect of sample volume on soil NO_3–N and soil moisture content. At all locations, soil samples were taken to a depth of 150 cm at 30 cm intervals by using each of the four sampling devices adjacently. Sampling was conducted beginning 3 June and continuing through 16 June, thus minimizing temporal variability among samples. A small rain shower (2 mm) on the afternoon of 11 June interrupted sampling, but rainfall amount was intercepted entirely by the crop canopy. The seasonal charts of events before and during the soil sampling including daily precipitation, fertilization, daily tile flow and its NO_3–N concentration are presented in Fig. 2.

Soil samples were analyzed for NO_3–N concentration and moisture content, resulting in (175 sites $\times$ 4 sampling methods =) 700 paired data. Each soil sample represents the average level of NO_3–N over 10 cm depth at a particular spatial location (x,y,z). A sample

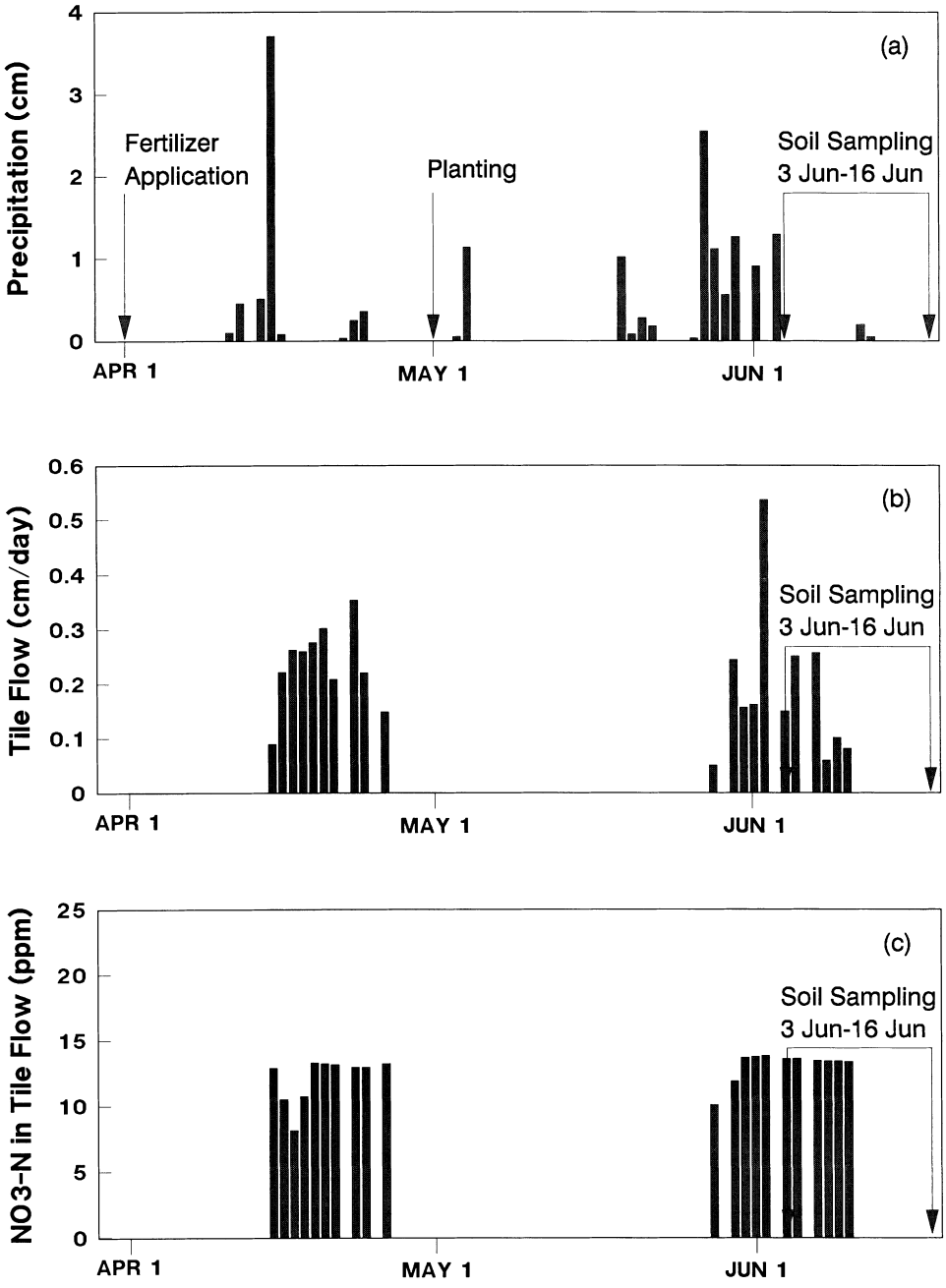

Fig. 2. Seasonal precipitation (a), tile outflow (b), and nitrate concentration of the tile effluent (c), in the experimental plot during and before the soil sampling event.

of 10 cm length was considered a point sample for the semivariogram or cross semivariogram estimation in horizontal (x- and y-) directions. However, semivariograms and cross semivariograms in the vertical (z-) direction were regularized (Journel and Huijbregts, 1978, pp. 79–85) to account for the sample length. Colorimetric automated cadmium reduction method (EPA 353.2) was used to determine the NO_3–N concentration in the soil sample. Soil moisture contents were determined gravimetrically and subsequently converted to volumetric values based on actual data-support for spatial analyses. Note that because same soil samples were used for determining both random functions, they could be called jointly located samples.

3. Knowledge-based spatial analysis

Mohanty and Kanwar (1994) presented a 'generic' scheme to analyze the three-dimensional spatial data arranged on a regular grid subjected to various directional trends because of different intrinsic and/or extrinsic factors. This analytical scheme is useful when we do not know exactly the factors that contribute to the spatial variability of the regionalized variable(s). With the repeated median polishing steps, we can remove the directional components leaving the random component behind. This can then be analyzed further for the field-inherent spatial variability of the regionalized variable(s).

In this paper we present a 'knowledge-based' spatial analysis scheme when the major component of the flow and transport (processes) that induces spatial nonstationarity in the regionalized variable(s) in the soil profile is known and can be characterized spatially. In the tile-drained soil profile, over years of cropping, fertilizer application, and seasonal precipitation, when we sample the soil profile for NO_3–N concentration and moisture content, these spatial data represent the joint output of various physical, chemical and biological processes over space and time including concurrent events. Fig. 2 shows the precipitation, tile flow rate, and NO_3–N concentration in the tile flow during the crop planting season which includes the 14 day long soil sampling window. Examination of Fig. 2(b) revealed that the soil sampling window included (1) an initial phase of saturated (tile) flow because of the rainfall before the sampling event, and (2) a second phase of no tile flow (i.e. variably saturated flow) in the soil profile. The initial saturated (tile) flow flushed out a large amount of NO_3–N (Fig. 2(c)). Subsurface-drain-induced flow under saturated condition can be mathematically quantified as Darcy-flux density ($q_{x,y,z}$) and spatially characterized at different soil layers and distances relative to the tile drain location. Variability in ($q_{x,y,z}$) relates to variability in saturated hydraulic conductivity ($K_{s\,x,y,z}$) and hydraulic gradient ($i_{x,y,z}$). Thus, point samples of NO_3–N concentration and moisture content need to be relative-flux-corrected to remove tile-drainage-induced nonstationarity before the 3-D spatial analysis. After relative-flux-correction, the residuals would represent the contribution from variably-saturated flow and the consequent NO_3–N transport in addition to the contribution from other physical, chemical, and biological factors.

Fig. 3(a) shows idealized flow-paths under equilibrium (steady state) saturated flow and mass transport in the vertical cross section of a tile-drained, layered soil profile (after Smedema and Rycroft, 1983, pp. 129–139). Converging flow paths or stream lines are

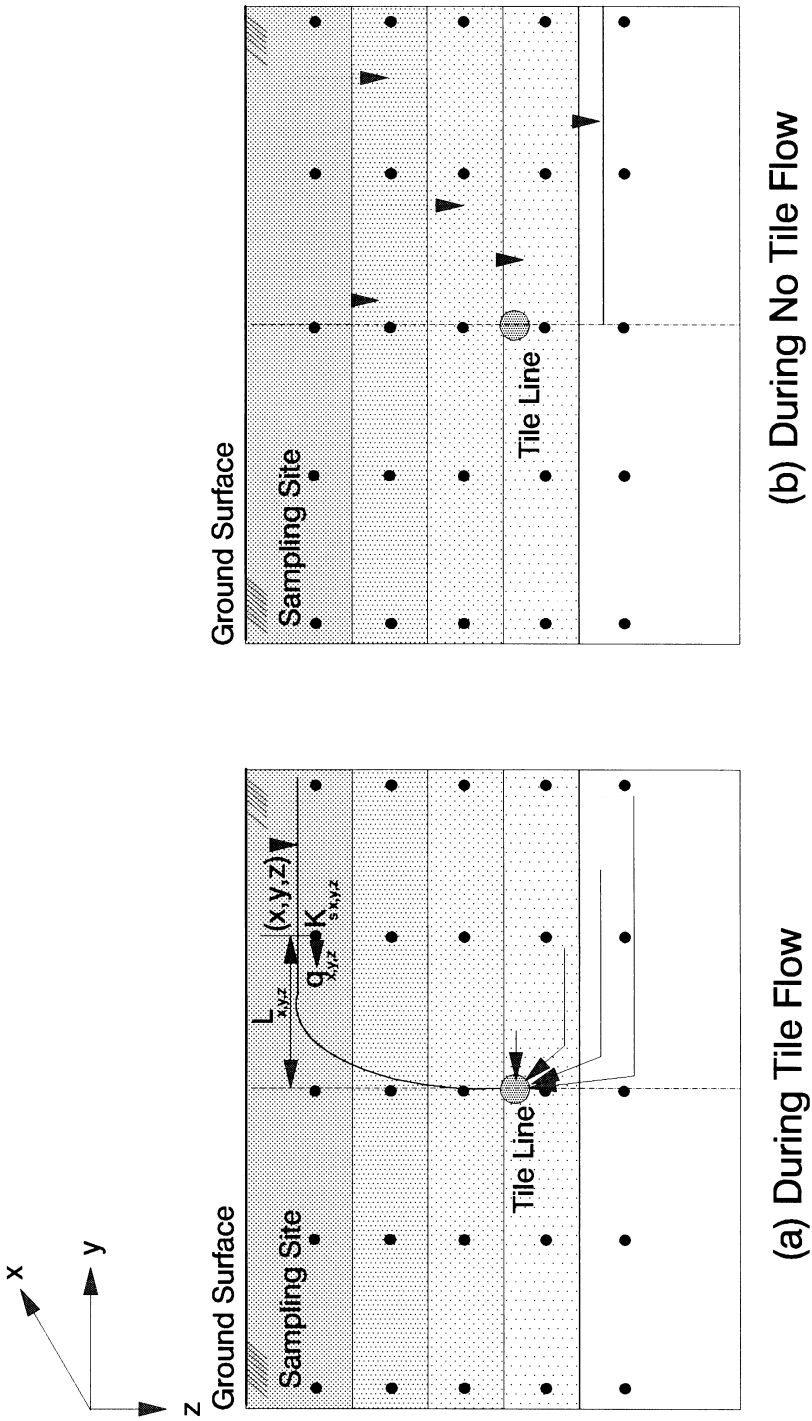

Fig. 3. Idealized saturated (a) and unsaturated (b) flow-paths in a tile-drained plot (after Smedema and Rycroft, 1983). Markers indicate the sampling locations in a vertical cross section of the soil profile.

perpendicular to the equipotential lines around the tile line, where the tile line represents the zero (i.e. atmospheric) pressure. Assuming horizontal and radial flow to tile (i.e. head loss owing to vertical flow usually being insignificant), the steady state flow in each layer can be described mathematically by a simple Hooghoudt formula (based on Darcy's law) (Smedema and Rycroft, 1983, pp. 139). By definition,

$$q = \frac{8K_s dh}{L^2} \tag{1}$$

where, q = tile discharge (LT^{-1}); K_s = horizontal saturated hydraulic conductivity (LT^{-1}); L = spacing between adjacent tiles (or field length perpendicular to the tile line contributing to tile flow, q) (L); h = head loss (across field length perpendicular to the tile line contributing to the tile flow, q) (L); d = thickness of equivalent horizontal flow zone below the tile drain (L).

Although tile flow was transient during the soil sampling event, to make a simple, yet reasonable analysis based on the available information, we assumed steady horizontal flow condition persists in the system during the tile flow (i.e., constant hydraulic gradient ($i = h_{x,y,z}/L_{x,y,z}$) for *each layer* and using average $\bar{K}_s$ for the layer). And adapting Eq. (1) for tile flow calculation, the relative-local-Darcy-flux-contribution ($q^r_{x,y,z}$) from different spatial location (x, y, z) to the tile discharge (q) will depend on ($K_{s\,x,y,z}$) and ($d_{L\,x,y,z}/L_{x,y,z}$). Intuitively, $d_{L\,x,y,z}$ is the thickness of equivalent horizontal flow length below the tile drain when $L_{x,y,z}$ is the contributing field length perpendicular to the tile line in y-direction and is equal to the radial distance close to tile line. Mathematically,

$$q^r_{x,y,z} \propto K_{s\,x,y,z} \tag{2}$$

and

$$q^r_{x,y,z} \propto \frac{d_{L_{x,y,z}}}{L_{x,y,z}} \tag{3}$$

When there is no distinct impermeable substratum, as in our study site, $d_{L\,x,y,z}$ will remain (roughly) constant for all $L_{x,y,z}$ (Smedema and Rycroft, 1983). Thus (2) and (3) can be simplified,

$$q^r_{x,y,z} \propto \frac{K_{s\,x,y,z}}{L_{x,y,z}} \tag{4}$$

To remove drainage-induced variability, moisture content ($\theta_{x,y,z}$) and residual NO_3–N concentration ($N_{x,y,z}$) were proportioned by relative-local-Darcy-flux-density ($q^r_{x,y,z}$) contributing to the tile flow. Dimensionless relative values of saturated hydraulic conductivity ($K^r_{s\,x,y,z}$) and length ($L^r_{x,y,z}$) were used to calculate the dimensionless relative-local-Darcy-flux density ($q^r_{x,y,z} = K^r_{s\,x,y,z}/L^r_{x,y,z}$) contributing to the tile flow. $K^r_{s\,x,y,z}$ is defined as the ratio of horizontal saturated hydraulic conductivity ($K_{s\,x,y,z}$) at location (x,y,z) to the 3-D average horizontal saturated hydraulic conductivity (K_s 3D). $L^r_{x,y,z}$ is the ratio of horizontal distance (in y-direction) of location (x,y,z) from the tile line to the length of the experimental plot. For locations close to the tile line (e.g. above or below the tile line)

$L_{x,y,z}$ is approximated with the radial distance. Thus relative-flux-corrected NO_3–N concentration and relative-flux-corrected moisture content for this study are defined as:

$$\hat{N}_{x,y,z} = N_{x,y,z} * q^r_{x,y,z} \tag{5}$$

$$\hat{\theta}_{x,y,z} = \theta_{x,y,z} * q^r_{x,y,z} \tag{6}$$

where, $\hat{N}_{x,y,z}$ = relative-flux-corrected nitrate concentration at spatial location (x,y,z); $N_{x,y,z}$ = soil water nitrate concentration at spatial location (x,y,z); $\hat{\theta}_{x,y,z}$ = relative-flux-corrected soil moisture content at spatial location (x,y,z); $\theta_{x,y,z}$ = soil moisture content at spatial location (x,y,z); $q^r_{x,z,y}$ = relative-local-Darcy-flux-density at spatial location (x,y,z) contributing to tile-flow.

For completeness, a sample calculation of relative-flux-correction parameter is shown in the appendix.

$K_{s\ x,y,z}$ may be random or spatially correlated in the 3-D soil profile. Moreover, correlation scale of $K_{s\ x,y,z}$ may be anisotropic in horizontal and vertical directions (Dagan, 1989). Researchers more often claim that the correlation length for $K_{s\ x,y,z}$ is smaller in the vertical direction than in horizontal directions. This may be because of the soil layering across depth direction that are deposited during different geological time under different depositional processes, composed of different parent materials, and subjected to different stress, resulting in varying soil hydraulic properties. To address the variability of $K_{s\ x,y,z}$ in relative-local-Darcy-flux-density for steady horizontal flow to tile line, we measured K_s at five (30, 60, 90, 120 and 150 cm) depths at five different sites in the field and assumed that average $\bar{K}_s$ is homogenous and isotropic in each horizontal layer. Although homogeneity and isotropicity assumptions are rare in most field soils including ours, we adopted them to simplify our plot-scale problem. In a large field this method may loose its advantage because of the same reason. K_s was measured in undisturbed 7.6 cm diameter and 7.6 cm long vertical soil cores extracted from 30, 60, 90, 120 and 150 cm depths, using a constant head permeameter in the laboratory.

After tile-induced nonstationarity was removed from the spatial data, NO_3–N concentration and moisture content data were analyzed for spatial variability and possible coregionalization in 3-D. Semivariogram (used for kriging) and cross semivariogram (used for cokriging) (Journel and Huijbregts, 1978) are briefly described in the following section.

In geostatistics, semivariogram (γ^*) function gives a measure of how well a random variable (Z_n) is correlated in space as a function of the separation distance (h). By definition,

$$\gamma^*(\boldsymbol{h}_\alpha) = \frac{1}{2N(\boldsymbol{h}_\alpha)} \sum_{i=1}^{N(\boldsymbol{h}_\alpha)} [z_1(x_i) - z_1(x_i + \boldsymbol{h}_\alpha)]^2 \tag{7}$$

where $N(\boldsymbol{h}_\alpha)$ is the number of pairs of values $(z_1(x_i), z_1(x_i + \boldsymbol{h}_\alpha)$, separated by a vector h. As with any vectorial function, $\gamma^*(\boldsymbol{h}_\alpha)$ depends on both the magnitude ($|\boldsymbol{h}|$) and the direction (α) of $\boldsymbol{h}$ between the sample pairs. Dependency of the semivariogram on the direction (α) is known as the condition of anisotropy.

Just as values of a property (random variable) can depend in the statistical sense on

those of the same property at other nearby locations, so can they be related spatially to values of other property(ies) (random variable(s)). If so, the variables are said to be coregionalized. By analogy, the coregionalization of the primary variable (Z_1) and a covariable (Z_2) can be expressed by a cross semivariogram γ^*_{12} or γ^*_{21} defined as

$$\gamma^*_{12}(\boldsymbol{h}_\alpha) = \gamma^*_{21}(\boldsymbol{h}_\alpha) = \frac{1}{2N(\boldsymbol{h}_\alpha)} \sum_{i=1}^{N(\boldsymbol{h}_\alpha)} [z_1(x_i) - z_1(x_i + h_\alpha)][z_2(x_i) - z_2(x_i + h_\alpha)] \tag{8}$$

where $N(\boldsymbol{h}_\alpha)$ is the number of pairs of values $[z_1(x_i),\ z_1(x_i + \boldsymbol{h}_\alpha)]$ $[z_2(x_i),\ z_2(x_i + \boldsymbol{h}_\alpha)]$ separated by vector $\boldsymbol{h}$. As semivariograms, cross semivariograms could be checked for anisotropy. Cross semivariograms are anisotropic, particularly when the semivariograms are so. Researchers have pointed out that the use of cross semivariograms is not productive unless two regionalized variables are significantly correlated and have well-structured semivariogram. In a 3-D context, spatial variability of two correlated regionalized variables (Z_1 and Z_2) can be described with composite three-dimensional semivariograms and composite three-dimensional cross semivariogram (Myers and Journel, 1990). Mathematically,

$$\gamma_1(\boldsymbol{h}_x, \boldsymbol{h}_y, \boldsymbol{h}_z)^* = \overline{\gamma_1}(\boldsymbol{h}_x)^* + \overline{\gamma_1}(\boldsymbol{h}_y)^* + \overline{\gamma_1}(\boldsymbol{h}_z)^* \tag{9}$$

$$\gamma_2(\boldsymbol{h}_x, \boldsymbol{h}_y, \boldsymbol{h}_z)^* = \overline{\gamma_2}(\boldsymbol{h}_x)^* + \overline{\gamma_2}(\boldsymbol{h}_y)^* + \overline{\gamma_2}(\boldsymbol{h}_z)^* \tag{10}$$

$$\gamma_{12}(\boldsymbol{h}_x, \boldsymbol{h}_y, \boldsymbol{h}_z)^* = \overline{\gamma_{12}}(\boldsymbol{h}_x)^* + \overline{\gamma_{12}}(\boldsymbol{h}_y)^* + \overline{\gamma_{12}}(\boldsymbol{h}_z)^* \tag{11}$$

In Eqs. (9)–(11), sample semivariograms ($\bar{\gamma}^*_1$, $\bar{\gamma}^*_2$) and sample cross semivariograms ($\overline{\gamma}^*_{12}$) in *x*, *y*, and *z* directions are weighted averages over the 3-D sampling grid. As defined in Mohanty and Kanwar (1994), weighted semivariograms are calculated by using proportional weights based on number of sample pairs available at each lag distance over the 3-D soil volume. Semivariograms/cross semivariograms computation was made by using the geostatistical software package, GEOPACK (Yates and Yates, 1990).

4. Results and discussion

Means and variances of soil water NO_3–N concentration and volumetric moisture content for four sampling devices are presented in Table 1. Statistical comparison (Duncan's test) indicated significant differences (at $P = 0.99$) in soil water NO_3–N concentration because of difference in sample volume. Baker et al. (1989) has discussed the issue in detail for different tillage practices. Based on this finding, we limited our follow-up spatial analysis to one set of data collected from relatively smaller sample volumes to better represent the point data. Data collected by the 3.2 cm diameter soil probe were used for spatial analysis. Statistical measures of NO_3–N concentrations (in mg l^{-1}) and soil moisture contents (in cm) including mean, standard deviation, coefficient of variation, and range at different depths measured by a 3.2 cm diameter soil probe are presented in Table 2 for comparison purposes. Results show a consistent decrease in nitrate levels to a depth of 90 cm and then re-accumulation and more stable distribution of NO_3–N between 90 and 150 cm. For soil moisture content, although no specific trend was found in mean values

Table 1
Means and variances of soil water NO_3–N concentration and soil moisture content as a function of sample diameter

Depth cm	Device diameter (cm)							
	1.9		3.2		5.1		20.3	
	mean	variance	mean	Variance	mean	variance	mean	variance
	Soil Water NO_3–N (mg l^{-1})							
30	13.5	43.0	19.4	189.4	22.8	192.6	18.9	112.6
60	12.9	27.4	14.4	45.6	16.1	44.9	16.5	67.2
90	8.8	16.6	8.2	7.9	9.4	13.6	11.4	9.1
120	9.8	8.7	10.5	15.0	10.6	7.4	11.5	8.3
150	12.0	7.2	11.8	5.9	12.3	6.3	12.2	5.3
	Soil Moisture Content (cm)							
30	3.06	0.14	2.96	0.08	3.13	0.08	2.96	0.09
60	3.13	0.11	3.16	0.17	3.2	0.13	3.2	0.10
90	2.7	0.19	2.73	0.18	2.73	0.18	2.66	0.16
120	2.96	0.22	3.03	0.22	2.83	0.22	3.03	0.24
150	3.30	0.32	3.50	0.34	3.36	0.48	3.63	0.32

with the change of depth, the coefficient of variation showed a small increasing trend with depth. But the spatial variation of soil moisture content became very stable for depths below 90 cm. Average saturated hydraulic conductivities ($\bar{K}_s$) measured at five (0, 30, 60, 90, 120 and 150 cm) depths are presented in Table 3. Increase in $\bar{K}_s$ was observed from shallow to deeper depths. The trend in $\bar{K}_s$ across depth was opposite to that of soil water NO_3–N concentration. This finding might suggest that higher conductivity at deeper depths causes larger removal of soluble NO_3–N from the soil profile to the tile water in comparison with shallower depths during occasional buildup of shallow water tables, which leaves very little residual NO_3–N at the deeper soil depths.

Drainage-induced nonstationarity in the mean and the variance of the regionalized variables was removed, incorporating the relative-local-Darcy-flux based correction. With Shapiro–Wilk *w*-statistics, relative-flux-corrected NO_3–N concentration and relative-flux-corrected moisture content were found to be described by log-normal distribution at ($P = 0.10$) level. In Fig. 4, mean versus variance plots illustrate the improvement of constancy of variance after the $\log_e$-transformation with relative-Darcy-flux based correction compared with the raw data. Thirty five data points were gathered by taking mean and variance for 35 sampling holes. Except for data points adjacent to the tile line, the mean and the variance across holes showed apparent constancy. Thus, all further spatial analyses were carried with $\log_e$-transformed relative-flux-corrected data, excluding those adjacent to the tile line. Log_e-transformed relative-flux-corrected data of soil water NO_3–N concentration and soil moisture content were also examined for spatial correlation in the 3-D soil profile. Fig. 5 shows high positive spatial correlation ($r = 0.96$) between the loge-transformed relative-flux-corrected NO_3–N concentration and loge-transformed relative-flux-corrected moisture content data over the 3-D soil profile. Moreover, Fig. 5 shows the

Table 2
Statistical moments of soil water nitrate concentration and soil moisture content measured using 3.2cm diameter soil probe

	NO_3–N Conc. (mg l^{-1})	Moisture Content (cm)
	Depth = 30 cm	
Mean	19.340	2.96
Minimum	5.500	2.20
Maximum	83.300	3.61
Variance	189.4	0.08
No Sample	35	35
	Depth = 60 cm	
Mean	14.386	3.16
Minimum	7.200	2.38
Maximum	38.800	4.25
Variance	45.6	0.17
No Sample	35	35
	Depth = 90 cm	
Mean	8.157	2.73
Minimum	3.500	2.23
Maximum	14.200	4.04
Variance	7.9	0.18
No Sample	35	35
	Depth = 120 cm	
Mean	10.191	3.03
Minimum	4.900	2.39
Maximum	22.300	4.28
Variance	15.0	0.22
No Sample	35	35
	Depth = 150 cm	
Mean	11.846	3.50
Minimum	6.600	2.38
Maximum	17.700	5.13
Variance	5.9	0.34
No Sample	35	35

Table 3
Measured saturated hydraulic conductivity as a function of depth

Depth (cm)	Saturated Hydraulic Conductivity* (cm/day)		
	Mean	Max	Min
30	5.2	15.3	3.2
60	18.3	43.2	10.5
90	79.0	120.3	65.0
120	66.5	100.2	47.6
150	94.4	142.5	77.9

*K_s measured at 5 different sites across the plot.

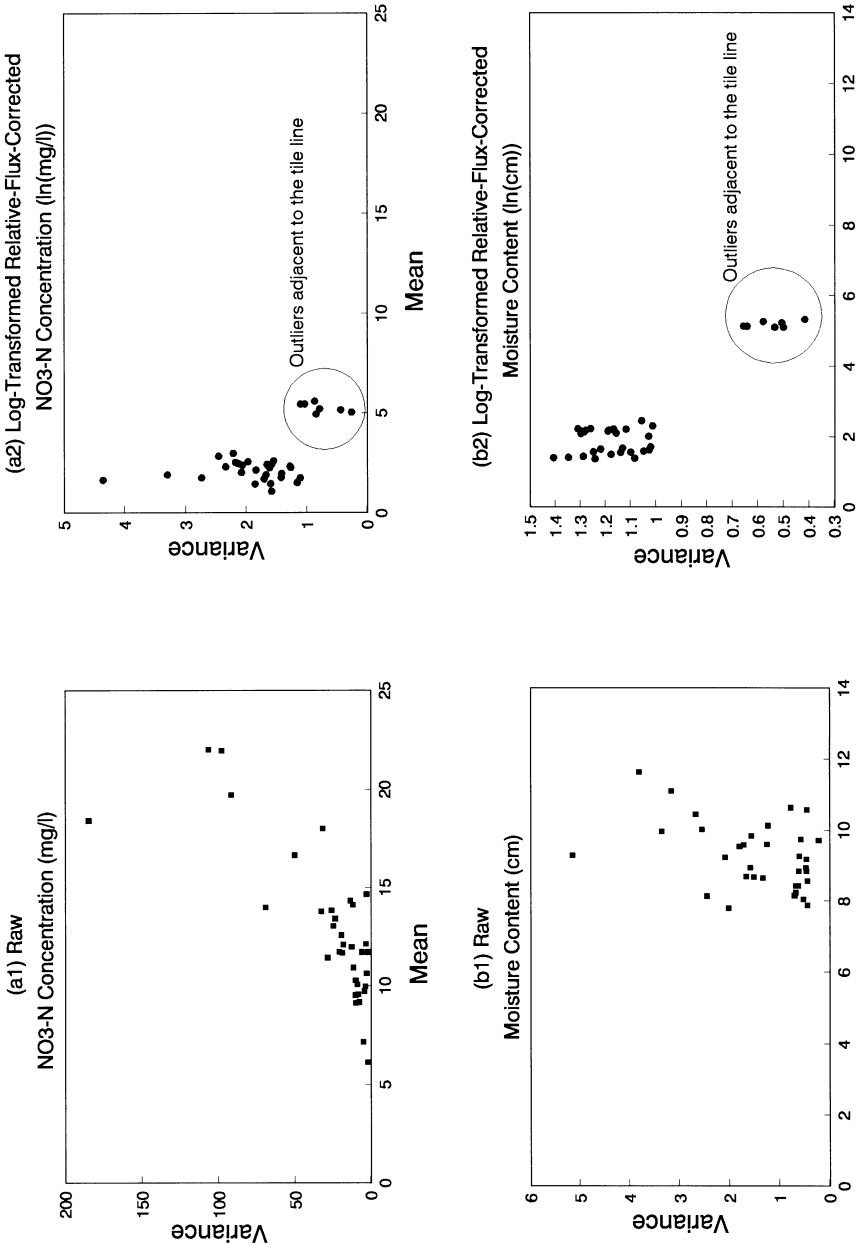

Fig. 4. Check for nonstationarity in the variance. Variance vs. mean (spread vs. level) plots of raw (1) and $\log_e$-transformed relative-flux-corrected (2) soil water NO_3–N concentration (a) and soil moisture content (b).

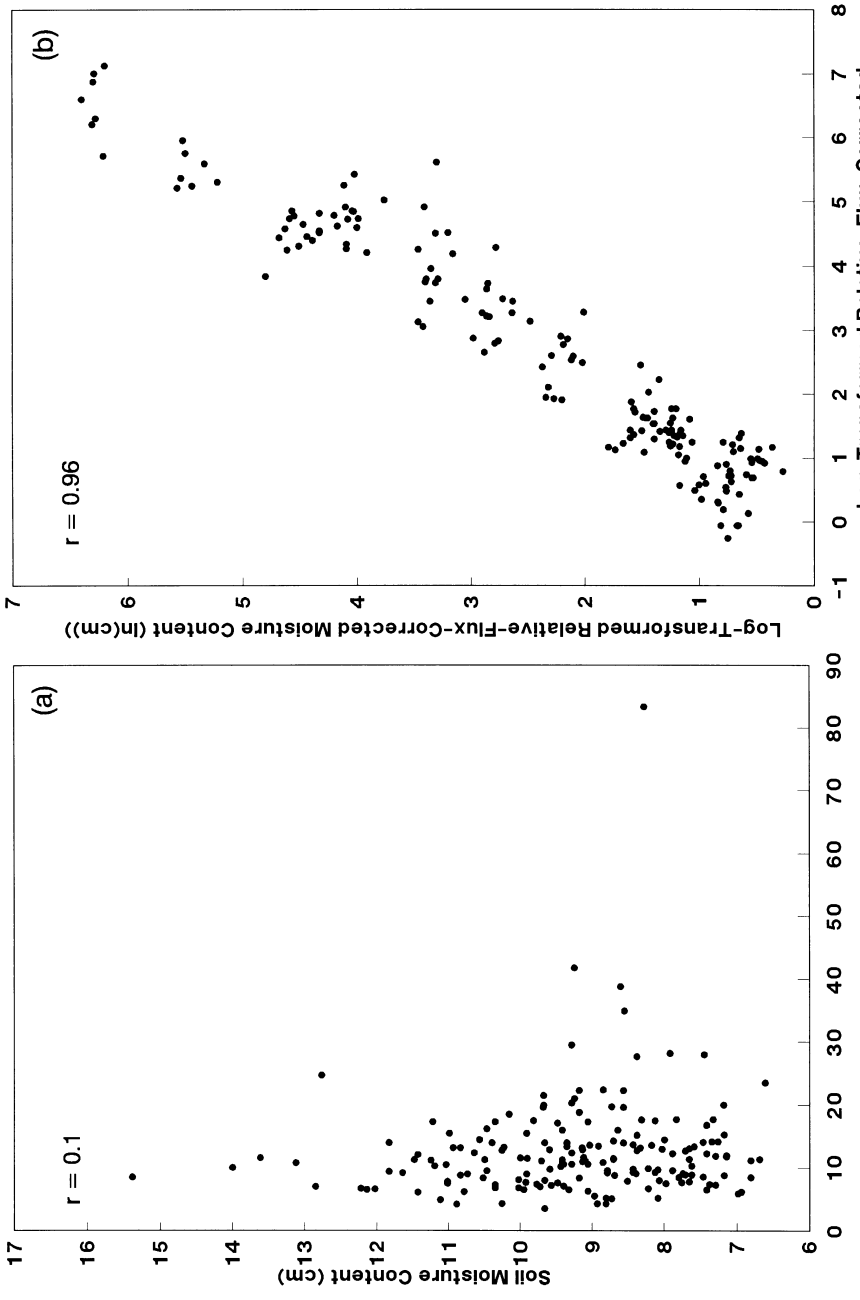

Fig. 5. Correlation plots (a) raw NO_3–N concentration and raw soil moisture content, and (b) $\log_e$-transformed relative-flux-corrected NO_3–N concentration and $\log_e$-transformed relative-flux-corrected soil moisture content.

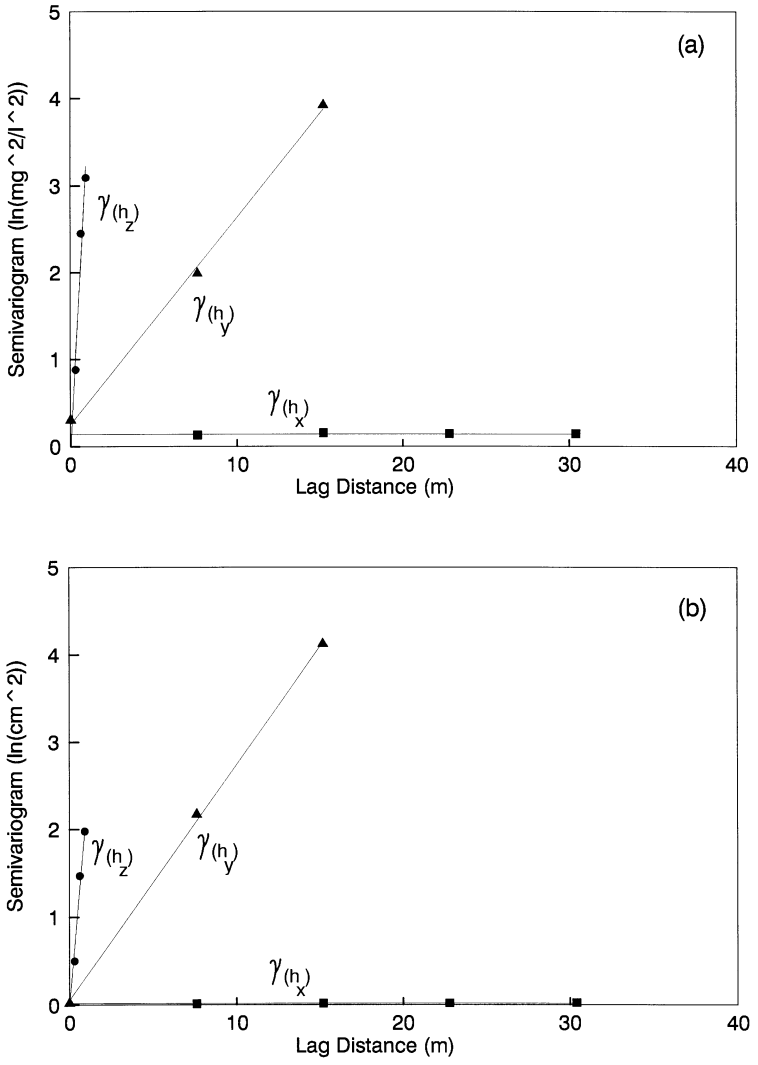

Fig. 6. Experimental 3-D composite semivariogram with fitted theoretical models for $\log_e$-transformed relative-flux-corrected NO_3–N concentration (a) and $\log_e$-transformed relative-flux-corrected soil moisture content (b).

large improvement of correlation coefficient after adopting relative-flux-correction in comparison with that for raw data. It is, however, important that precaution should be taken for any reverse analysis and interpretation (i.e. from relative-flux-corrected variables to actual variables) resulting from any spurious correlation.

Experimental directional-semivariograms in *x*-, *y*-, and *z*-directions were estimated for $\log_e$-transformed relative-flux-corrected NO_3–N concentration and $\log_e$-transformed relative-flux-corrected moisture content. Because we used a compact 3-D rather than a distributed 2-D spatial grid, each directional semivariogram was limited up to three quarter of

Table 4
Summary of 3-D composite semivariogram and 3-D composite cross semivariogram models. Models were cross-validated by jackknifing approach

Principal direction	Model	R_μ	$R_{\sigma 2}$
	Semivariogram model for log-transformed relative-flux-corrected NO_3–N concentration ($\ln(mg^2\ l^{-2})$)		
x-	$\gamma_1(\boldsymbol{h}_x) = 0.135$		
y-	$\gamma_1(\boldsymbol{h}_y) = 0.256 + 0.238\boldsymbol{h}_y$	0.016	1.09
z-	$\gamma_1(\boldsymbol{h}_z) = 3.58\boldsymbol{h}_z$	0.02	1.12
z-(regularized)	$\gamma_1(\boldsymbol{h}_z) = 3.58\boldsymbol{h}_z - 0.033$		
	Semivariogram model for log-transformed relative-flux-corrected moisture content ($\ln(cm^2)$)		
x-	$\gamma_2(\boldsymbol{h}_x) = 0.0198$		
y-	$\gamma_2(\boldsymbol{h}_y) = 0.0525 + 0.269h_y$	0.015	1.11
z-	$\gamma_2(\boldsymbol{h}_z) = 2.23\boldsymbol{h}_z$	0.018	1.19
z-(regularized)	$\gamma_2(\boldsymbol{h}_z) = 2.23\boldsymbol{h}_z - 0.033$		
	Cross semivariogram model for log-transformed relative-flux-corrected NO_3–N concentration and log-transformed relative-flux-corrected moisture content ($\ln(cm\ mg^{-1}\ l^{-1})$)		
x-	$\gamma_{12}(\boldsymbol{h}_x) = -0.0192$		
y-	$\gamma_{12}(\boldsymbol{h}_y) = -0.008 + 0.259\boldsymbol{h}_y$	0.027	1.02
z-	$\gamma_{12}(\boldsymbol{h}_z) = 2.736h_z$	0.009	1.10
z-(regularized)	$\gamma_{12}(\boldsymbol{h}_z) = 2.736\boldsymbol{h}_z - 0.033$		

the maximum lag distance in the respective direction. Moreover, considering the spatial symmetry of the plot across the tile line in *y*-direction, the semivariogram at $\boldsymbol{h}_y$ equal to zero is equivalent to the semivariogram for $\boldsymbol{h}_y$ equal to the length of the tile-drained plot. Weighted-average directional semivariograms ($\bar{\gamma}\ (\boldsymbol{h}_x)^*$, $\bar{\gamma}\ (\boldsymbol{h}_y)^*$, $\bar{\gamma}\ (\boldsymbol{h}_z)^*$) were calculated in *x*-, *y*-, and *z*-directions to compose the 3-D semivariograms for the soil profile (Fig. 6). Of the 3-D composite semivariogram, each directional semivariogram (estimation) was based on a maximum of 150 to a minimum of 50 lag pairs at different lag distances. Semivariograms for relative-flux-corrected NO_3–N concentration and relative-flux-corrected moisture content showed anisotropic linear structures (within the specified lag). We suggest that the anisotropic feature in *x*- versus *y*-semivariograms may be owing to untreated temporal-nonstationarity (because of transient tile flow in *y*-direction) during the soil sampling event. Considering the spatial structures and strong spatial correlation between relative-flux-corrected NO_3–N and relative-flux-corrected moisture content, a 3-D composite cross semivariogram was calculated and is presented in Fig. 7. Inasmuch as the correlation coefficients between these two functions are good, the cross-semivariogram structures depend only on the structures of the component semivariograms. Therefore, the cross semivariograms were linear, however, anisotropic in *x*-, *y*-, and *z*-directions. The highest slope was observed in *z*-direction, the lowest in *x*-direction, and the intermediate in *y*-direction. Linear models and/or nuggets could describe these 3-D composite semivariograms and 3-D composite cross semivariograms very well. Parameters of the fitted models are given in Table 4. Models in *z*-direction, however, were

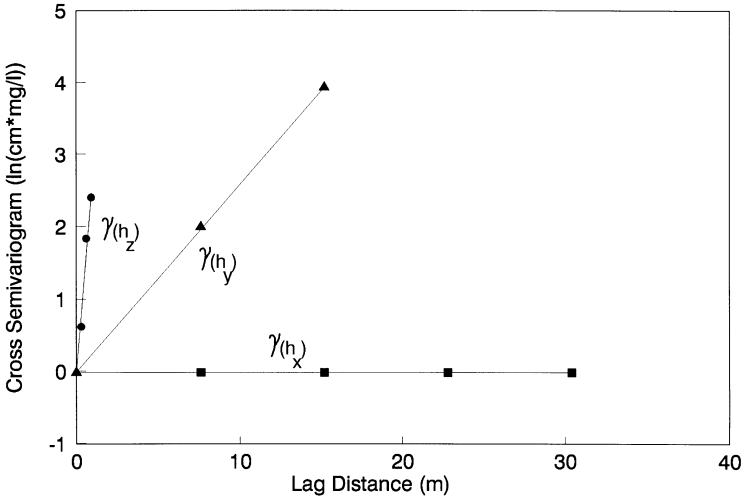

Fig. 7. Experimental 3-D composite cross semivariograms between $\log_e$-transformed relative-flux-corrected NO_3–N concentration and $\log_e$-transformed relative-flux-corrected soil moisture content with fitted theoretical models.

regularized to account for the sample length. The mean reduced error R_μ and associate reduced variance $R_{\sigma 2}$, (Vauclin et al., 1983) values for each semivariogram and cross semivariogram models are reported in Table 4 and should be approximately 0 and 1, respectively. No defined range, however, is developed to justify its validity.

These 3-D composite cross semivariograms would save lot of time and money when more expensive random components (relative-flux-corrected) soil water NO_3–N concentration could be predicted by a cheap surrogate such as (relative-flux-corrected) soil moisture content at locations where NO_3–N concentration is not measured. Similar knowledge-based adaptive spatial analysis techniques could be developed and implemented for other site-specific spatial problems.

5. Summary

Soil water NO_3–N concentration and soil moisture content data collected from 175 sites arranged on a $(5 \times 7 \times 5)$ 3-D grid of regular grid spacings (7.6 m × 7.6 m × 0.3 m) in a tile-drained soil profile under a conventional tillage agricultural plot in central Iowa were analyzed for spatial structure. As under subsurface tile flow condition, NO_3–N distribution in the soil profile is correlated to that of the tile-induced flux density and resident soil moisture content, a simple relative-local-Darcy-flux-correction scheme was adapted to remove the relative-flux-variability and thus drainage-induced nonstationarity in the spatial data. Follow up spatial analyses discovered anisotropic linear structures in the composite semivariograms (of $(\bar{\gamma}\ (\boldsymbol{h}_x)^*$, $\bar{\gamma}\ (\boldsymbol{h}_y)^*$, and $\bar{\gamma}\ (\boldsymbol{h}_z)^*)$ for relative-flux-corrected NO_3–N concentration and relative-flux-corrected moisture content in the 3-D soil profile. Anisotropic linear structures of 3-D composite semivariograms of relative-flux-corrected

NO_3–N concentration and relative-flux-corrected moisture content and their good spatial correlation resulted in 3-D anisotropic linear cross semivariograms. These 3-D composite cross semivariograms would be more economical when more expensive and labor-intensive data sets on (relative-flux-corrected) NO_3–N concentrations could be predicted with a cheap surrogate predictor such as the measured (relative-flux-corrected) soil moisture content, at unsampled locations.

Acknowledgements

This project was partly funded by Iowa Department of Natural Resources through grant support.

Appendix A. Calculation of Relative-Flux-Correction Parameter

Suppose the tile line is located along the x-axis at (x,0,0) in a three-dimensional grid. Then the relative-flux correction at a point (x,y,z) will be calculated using the following steps:

(i) dimensionless relative saturated hydraulic conductivity, $K^r_{x,y,z}$, at (x,y,z)

$$K^r_{x,y,z} = \frac{K_{s\,x,y,z}/\overline{K_{s,3D}}}{\sum_{y,z}(K_{s,x,y,z}/\overline{K_{s,3D}})} \tag{12}$$

where $K_{s\,x,y,z}$ and $\overline{K}_{s\,3D}$ are saturated hydraulic conductivity at (x,y,z) and geometric mean saturated hydraulic conductivity across the three-dimensional study volume, respectively. When the saturated hydraulic conductivity is assumed to be homogenous in x and y directions summation in the denominator (12) is done in z direction only.

(ii) dimensionless relative distance from the tile line, $L^r_{x,y,z}$, at (x,y,z)

$$L^r_{x,y,z} = \sqrt{(y-0)^2+(z-0)^2}/L \tag{13}$$

where L is half-spacing between consecutive tiles or length of influence of the tile drain.

(iii) dimensionless relative-local-Darcy-flux-density, $q^r_{x,y,z}$, at (x,y,z) contributing to tile flow

$$q^r_{x,y,z} = K^r_{x,y,z}/L^r_{x,y,z} \tag{14}$$

These $q^r_{x,y,z}$ were subsequently used to remove (saturated) tile-flow induced nonstationarity in soil nitrate concentration and soil moisture content data using Eq. (5) and (6), respectively.

References

Ahmed, S. and De Marsily, G., 1987. Comparison of geostatistical methods for estimating transmissivity using data on transmissivity and specific capacity. Water Resour. Res., 23: 1717–1737.

Baker, D., Kanwar, R.S. and Baker, J.L., 1989. Sample volume effect on the determination of nitrate–nitrogen in the soil profile. Trans. ASAE, 32 (3): 934–938.

Baker, J.L., Campbell, K.D., Johnson, H.P. and Hanway, J.J., 1975. Nitrate, Phosphorous, and Sulfate in subsurface drainage water. J. Environ. Qual., 4: 406–412.

Beek, J. and Frissel, M.J., 1973. Simulation of nitrogen behavior in soils, PUDOC., Wageningen, The Netherlands.

Butters, G., Jury, W.A. and Ernst, R.F., 1989. Field scale transport of bromide in an unsaturated soil 1. Experimental methodology and results. Water Resour. Res., 25: 1575–1581.

Cressie, N.A.C., 1993. Statistics for Spatial Data, John Wiley, New York, 900 p.

Dagan, G., 1989. Flow and Transport in Porous Formations, Springer-Verlag, New York, 465 p.

Journel, A.G. and Huijbregts, C.J., 1978. Mining Geostatistics, Academic, New York, 600 p.

Kanwar, R.S., Johnson, H.P. and Baker, J.L., 1983. Comparison of simulated and measured nitrate losses in tile effluent. Trans. ASAE, 26 (5): 1451–1457.

Kanwar, R.S., Baker, J.L. and Baker, D.G., 1988. Tillage and split N-fertilization effects on subsurface drainage water quality and corn yield. Trans. ASAE, 31 (2): 453–460.

Kanwar, R.S. and Baker, J.L., 1991. Long-term effects of tillage and reduced chemical application on the quality of subsurface drainage and shallow groundwater. Proc. Environmentally Sound Agriculture, Orlando, Florida, pp. 121–129.

Mohanty, B.P., Kanwar, R.S. and Horton, R., 1991. A robust-resistant approach to interpret spatial behavior of saturated hydraulic conductivity of a glacial till soil under no-tillage system. Water Resour. Res., 27 (11): 2979–2992.

Mohanty, B.P. and Kanwar, R.S., 1994. Spatial variability of nitrate–nitrogen under conventional tillage vs no tillage—A composite 3-D resistant and exploratory approach. Water Resour. Res., 30 (2): 237–252.

Mohanty, B.P., Ankeny, M.D., Horton, R. and Kanwar, R.S., 1994a. Spatial analysis of hydraulic conductivity measured using disc infiltrometer. Water Resour. Res., 30 (9): 2489–2498.

Mohanty, B.P., Kanwar, R.S. and Everts, C.J., 1994b. Comparison of saturated hydraulic conductivity measurement methods for a glacial-till soil. Soil Sci. Soc. Am. J., 58 (3): 672–677.

Myers, D.E. and Journel, A.G., 1990. Variograms with zonal anisotropies and noninvertible kriging systems. Math. Geol., 22: 779–785.

Smedema, L.K. and Rycroft, D.W., 1983. Land Drainage, Batsford, London, 376 p.

Trangmar, B.B., Yost, R.S. and Uehara, G., 1986a. Spatial dependence and interpolation of soil properties in West Sumatra, Indonesia; I Anisotropic variation. Soil Sci. Soc. Am. J., 50: 1391–1395.

Trangmar, B.B., Yost, R.S. and Uehara, G., 1986b. Spatial dependence and interpolation of soil properties in West Sumatra, Indonesia; II Co-regionalization and Co-Kriging. Soil Sci. Soc. Am. J., 50: 1396–1400.

Vauclin, M., Vieira, S.R., Vachaud, G. and Nielsen, D.R., 1983. The use of cokriging with limited field soil observations. Soil Sci. Soc. Am. J., 47: 175–184.

Wagenet, R.J. and Rao, B.K., 1983. Description of nitrogen movement in the presence of spatially variable soil hydraulic properties. Agric. Water Manage., 6: 227–242.

White, R.E., Dyson, J.S., Haigh, R.A., Jury, W.A. and Sposito, G., 1986. Transfer function model of solute transport through soil, 2. Illustrative applications. Water Resour. Res., 22: 248–254.

Woodbury, A.D. and Sudicky, E.A., 1991. The geostatistical characteristics of borden aquifer. Water Resour. Res., 27: 533–546.

Yates, S.R. and Warrick, A.W., 1987. Estimating soil water content using cokriging. Soil Sci. Soc. Am. J., 51: 23–30.

Yates S.R., and Yates, M.V., 1990. United States Environmental Protection Agency, A user's manual for the GEOPACK (version 1.0) geostatistical software, EPA/600/8-90/004, 70 pp.